General Guided-Wave Impedance-Matching Networks with Waveguide-Metamaterial Elements

Wangyu Sun,[1] Xu Qin,[1] Shuyu Wang,[1] and Yue Li[1,2,*]

[1] *Department of Electronic Engineering, Tsinghua University, Beijing 100084, China*

[2] *National Research Center for Information Science and Technology, Beijing 100084, China*

(Received 3 June 2022; revised 26 July 2022; accepted 17 August 2022; published 26 September 2022)

A plasmonic based nanocircuit transplants the lumped property of classical electronic circuits to optical frequencies, providing a circuit paradigm for optics and photonics. To broaden the material and frequency selections, the concept of a waveguide metamaterial is applied to design lumped elements by utilizing the waveguide's structural dispersion to emulate the natural material's dispersion. Here, as an important application of the physics of waveguide metamaterials, a general type of impedance-matching network directly integrated with a waveguide is investigated for various matching occasions of guided waves, outperforming the classical ones using waveguide membranes. Three representative matching examples are analyzed to validate the feasibility, namely, transmission discontinuities, active power amplifiers, and antennas. The numerical and experimental results confirm the impedance-matching applications of the waveguide metamaterial and suggest the potential merits of low loss and low crosstalk for the proposed waveguide-integrated matching networks in terahertz integrated-circuit designs.

DOI: 10.1103/PhysRevApplied.18.034070

I. INTRODUCTION

The past decades have witnessed a boom in the development of metamaterials, which bring various exotic electromagnetic phenomena [1–5]. The plasmonic based nanocircuit, as a distinctive example of an application of a metamaterial, successfully transplants the notion of an electronic circuit into optical domains by exploiting plasmonic metamaterials to emulate the impedance properties of classical lumped elements [6,7], leading to a variety of intriguing nanocircuits for field and wave manipulation at the deep subwavelength scale [8–12]. To broaden the possibilities of this concept, the concept of the waveguide metamaterial is proposed. By utilizing the waveguide's structure dispersion instead of the natural plasmonic material's dispersion (i.e., Drude dispersion) [13], a waveguide with a regular material with positive permittivity inside can achieve an effective permittivity ranging from negative to positive, which is determined by the geometric size of the waveguide [14,15]. Based on the waveguide metamaterial, various interesting applications with versatile functions are proposed, including effective circuit elements [13], filters [16], and transmission structures [17,18]. The waveguide metamaterial extends the plasmonic based nanocircuit to the microwave and terahertz domains, where no natural plasmonic material exists, and avoids the intrinsic loss of natural plasmonic materials, promising high-efficiency plasmonic applications [19]. Furthermore, benefitting from the enclosed structure of the waveguide, these circuit applications realize much lower electromagnetic leakage and mutual coupling than that of classical microstrip-type integrated circuits, especially for terahertz or higher frequencies. The concept of a waveguide metamaterial has potential for various electromagnetic applications.

As an essential topic in engineering, impedance matching aims to eliminate the mismatch between source and load, minimizing the reflected power from the load and maximizing the transmitted power from the source [20,21]. To date, different types of impedance-matching networks have been constructed and utilized for various functionalities from microwave to optical frequencies, such as antennas [22,23], cloaking [24], absorbers [25], antireflection coatings [26], and power amplifiers [27]. Common matching networks utilize lumped circuit elements, i.e., capacitors and inductors, with the merit of subwavelength sizes. However, such a design is only feasible at lower microwave frequencies, due to the absence of lumped elements at terahertz and optical frequencies [20,21]. Additionally, conventional lumped elements are usually integrated with the microstrip-type structure, resulting in an unignorable radiation loss and crosstalk at higher frequencies. For other matching networks via periodical metamaterials or metasurfaces [28–32], they usually suffer from nonuniform structures and complicated design.

Here, we exploit the physics of the waveguide metamaterial to develop general impedance-matching

*lyee@tsinghua.edu.cn

 © 2022 American Physical Society

networks for guided waves. The impedance properties of the waveguide metamaterial are theoretically investigated and numerically verified. It is demonstrated that the dielectric layer inserted inside the waveguide behaves as an effective lumped capacitor or inductor when its effective permittivity is positive or negative. Using these waveguide-metamaterial (WG-MTM) lumped elements, general impedance-matching networks can be built and integrated with the waveguide to realize the impedance transformation between arbitrary sources and loads. On this basis, three proof-of-concept matching implementations are presented, i.e., matching networks for (i) transmission discontinuities, (ii) active power amplifiers, and (iii) radiating antennas. Compared with the microstrip-type networks, the proposed ones are able to perform over microwave to terahertz bands with lower loss and mutual couplings, which benefit from their enclosed structures. Moreover, different from the membrane-type waveguide-matching approach using higher-order-mode approximation [33], the proposed WG-MTM ones achieve single-mode operations, providing a different but better approach for terahertz integrated circuit designs.

II. CONCEPT AND THEORY

As conceptually depicted in Fig. 1(a), a general guided-wave matching network with WG-MTM elements is constructed for impedance matching between a load with a complex impedance of $Z_L = R_L + jX_L$ and a source with a real impedance of $Z_S = R_S$. The network is built within a regular metallic waveguide by inserting different dielectric layers [i.e., red parts in Fig. 1(b)] with subwavelength thicknesses, which behave as an emulation of classical lumped elements with a reactance of jX and are given the name "WG-MTM elements." Network sketches containing single, double, and triple elements with their equivalent-circuit models are presented in Figs. 1(b) and 1(c). In addition to the three examples in Figs. 1(b) and 1(c), the proposed concept is also applicable to other types of matching networks. In this manner, the general impedance-matching network has the potential to match arbitrary loads in various applications. Three representative forms (transmission discontinuity, an active power amplifier, and an antenna) are presented in Fig. 1(d), and they are numerically and experimentally validated in the following sections.

To begin with, the impedance properties of the waveguide metamaterial are investigated. As shown in Fig. 2(a), a WG-MTM element (dielectric layer in red) with the thickness of a is inserted inside a metallic rectangular waveguide operating at the TE_{10} mode. Supposing the actual relative permittivity of the background dielectric in the waveguide is ε_{WG}^{act} and the relative permittivity of WG-MTM element is ε_E^{act}, the waveguide's effective permittivities, ε_{WG}^{eff} and ε_E^{eff}, are calculated by [13]

$$\varepsilon^{eff} = (\pi c/w)^2/\omega^2 = \varepsilon^{act} - c^2/(4w^2 f_p^2) \quad (1)$$

where c is the speed of light in a vacuum, w is the width of the waveguide, f_p is the operating frequency, and ω is the angular frequency calculated by $\omega = 2\pi f_p$. By selecting appropriate parameters, the WG-MTM element has the ability to realize effective negative or positive permittivity, ε_E^{eff}. As demonstrated in Ref. [13], the effective capacitor and inductor model of the WG-MTM element are presented in Fig. 2(b). If $\varepsilon_E^{eff} > 0$, the element behaves as an effective parallel capacitor. If $\varepsilon_E^{eff} < 0$, the element behaves as an effective parallel inductor. Effective capacitance and

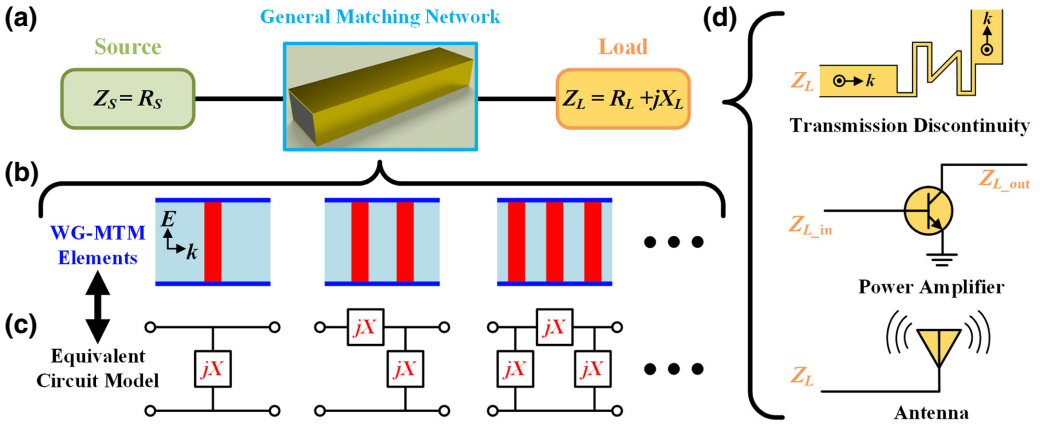

FIG. 1. General concept of a general guide-wave matching network with WG-MTM elements. (a) Sketch of the general matching network, which is introduced to match a load of arbitrary complex impedance with a source of arbitrary real impedance. (b) Network is developed by inserting some dielectric layers (i.e., red parts) inside the waveguide. These layers are given the name WG-MTM elements and can exhibit effective parallel or series reactance, jX. (c) Equivalent-circuit models of networks comprising single, double, triple, etc. WG-MTM elements. (d) Potential applications of impedance matching.

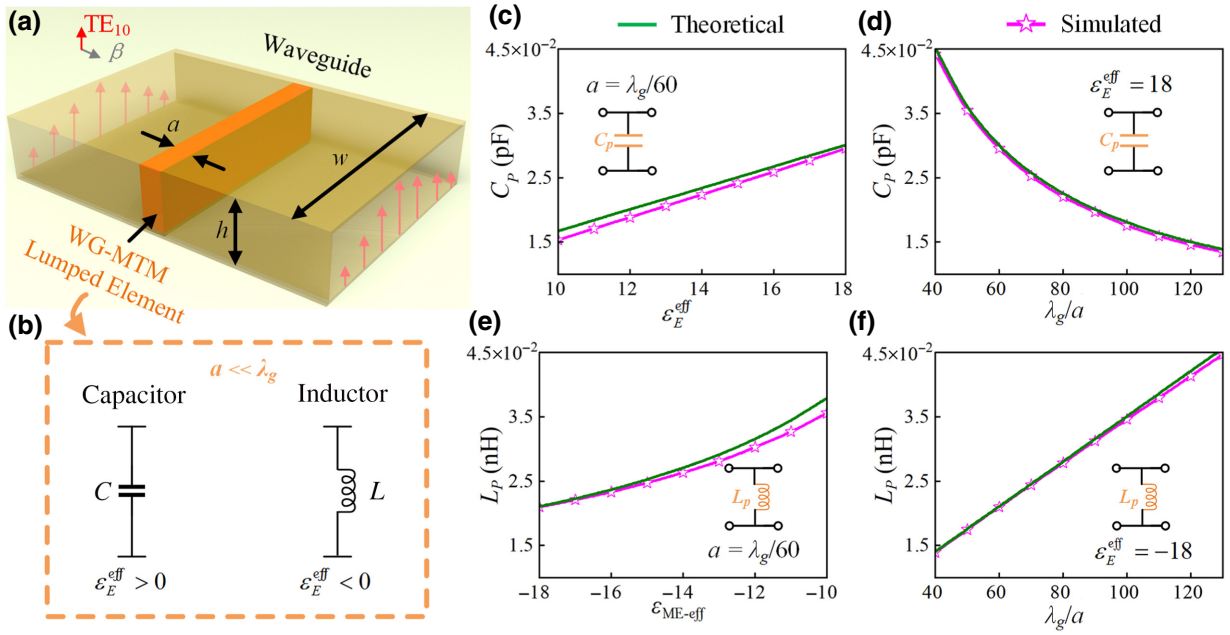

FIG. 2. Impedance properties of waveguide metamaterial. (a) Scheme of the WG-MTM element within a metallic rectangular waveguide. (b) Effective capacitor and inductor model of the WG-MTM elements. (c)–(f) Comparisons between theoretical and simulated parallel reactance (C_P or L_P) of WG-MTM elements. Effective capacitor, i.e., $\varepsilon_E^{\text{eff}} > 0$, (c) C_P vs $\varepsilon_E^{\text{eff}}$, and (d) C_P vs a. Effective inductor, i.e., $\varepsilon_E^{\text{eff}} < 0$, (e) L_P vs $\varepsilon_E^{\text{eff}}$ and (f) L_P vs a.

inductance are calculated by

$$C = a\varepsilon_E^{\text{eff}}\varepsilon_0\frac{Z_0}{Z_{\text{WG}}}, \tag{2}$$

$$L = -\frac{1}{4\pi^2 f_p^2 a\varepsilon_E^{\text{eff}}\varepsilon_0}\frac{Z_{\text{WG}}}{Z_0}. \tag{3}$$

Z_0 is the wave impedance in the waveguide, and Z_{WG} is the characteristic impedance [34,35]. In Ref. [13], Eqs. (2) and (3) are derived under the ideal epsilon-near-zero condition of $\varepsilon_{\text{WG}}^{\text{eff}} = 0$ (i.e., wavelength, λ_g, inside the waveguide is infinite) with an effective "static" but resonant field. Here, we discuss the feasibility of the waveguide metamaterial under the general condition of a guided wave. The effective permittivity of the background waveguide is set as $\varepsilon_{\text{WG}}^{\text{eff}} = 1$ and the guided wavelength is $\lambda_g = 1500$ μm at $f_p = 200$ GHz. The capacitance and the inductance with variation of $\varepsilon_E^{\text{eff}}$ and thickness, a, are investigated, as depicted in Figs. 2(c)–2(f). It is concluded that, in the guided-wave case, consistency between theoretical and numerical results can be obtained when the thickness of the WG-MTM element is on the subwavelength scale and $|\varepsilon_E^{\text{eff}}|$ has a large value. Detailed simulation configurations are presented in Fig. S1 within the Supplemental Material [36]. These results for WG-MTM elements of a guided wave provide guidelines for the construction of WG-MTM matching networks.

To highlight the advantage of the proposed WG-MTM element, comparisons of the matching performance with classical waveguide membranes [33] are investigated and presented in Fig. 3. Two metallic membranes along the y axis in Fig. 3(a) and the WG-MTM element with positive $\varepsilon_E^{\text{eff}}$ in Fig. 3(b) both behave as an effective capacitor to match the given impedance. Detailed structures and dimensions of Fig. 3 are presented in Figs. S2 and S3 within the Supplemental Material [36], respectively. Results in Fig. 3(c) indicate that the WG-MTM element achieves the −10-dB impedance bandwidth (i.e., frequency domains with a reflection coefficient lower than −10 dB) of 23.9% ($0.878f_p$–$1.117f_p$), which is much broader than 1.9% ($0.991f_p$–$1.009f_p$) realized by membranes. On the other hand, two metallic membranes along the x axis in Fig. 3(d) and the WG-MTM element with negative $\varepsilon_E^{\text{eff}}$ in Fig. 3(e) both behave as an effective inductor to match the situation requiring inductive impedance. The matching bandwidth obtained by the WG-MTM is 24.9% ($0.888f_p$–$1.14f_p$), outperforming the bandwidth of 9.8% ($0.953f_p$–$1.051f_p$) obtained for classical membranes, as shown in Fig. 3(f).

Comparing the matching performance between these two approaches in Fig. 3, the results of examples demonstrate that the proposed WG-MTM matching networks achieve a better matching property than regular waveguide membranes. As another difference, the WG-MTM matching network is designed with a single mode within the waveguide, without excitation of the higher-order mode of waveguide membranes. Additionally, the effects of material loss and metal loss on the performance of

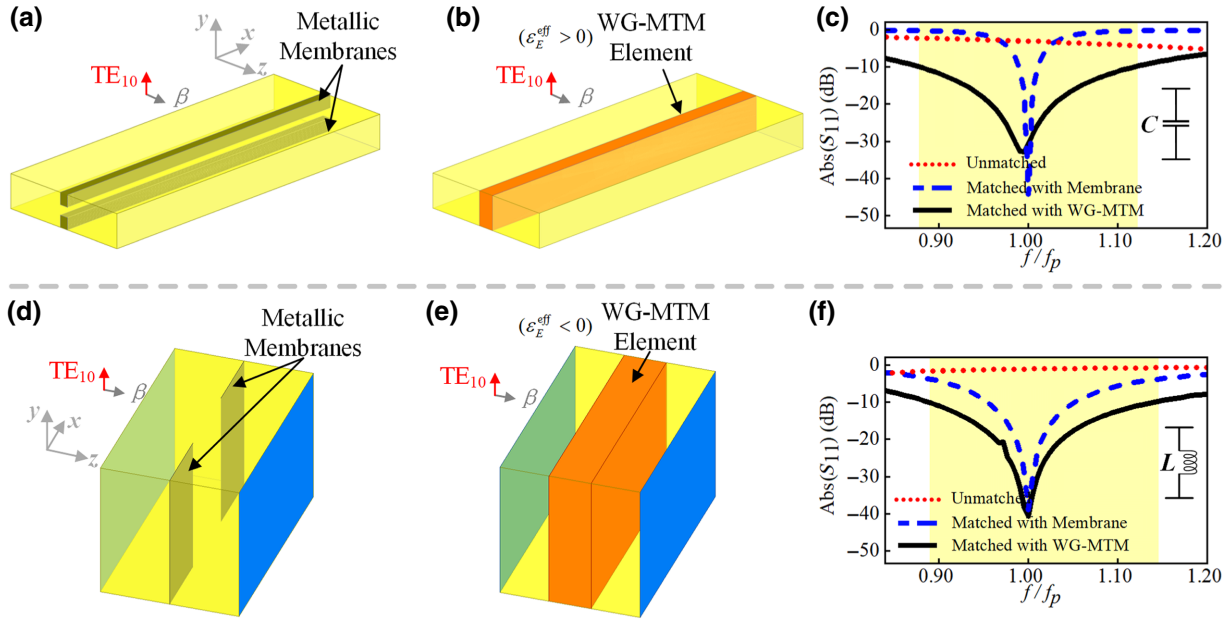

FIG. 3. Performance comparisons between waveguide metamaterial and classical metallic membranes. Scheme of the matching network with (a) capacitive waveguide metallic membranes or (b) capacitive WG-MTM element. (c) Reflection coefficients of (a),(b). Scheme of the matching network with (d) inductive waveguide metallic membranes or (e) inductive WG-MTM element. (f) Reflection coefficients of (d),(e).

the WG-MTM matching network are studied at terahertz frequency, as shown in Fig. S4 within the Supplemental Material [36]. Results indicate that the proposed concept has strong robustness against inevitable losses in actual applications. In the next part, three representative applications, i.e., transmission discontinuities, a power amplifier, and an antenna, are investigated to demonstrate the feasibility of general matching networks with waveguide metamaterial.

III. APPLICATIONS OF WG-MTM MATCHING NETWORKS

A. Matching for transmission discontinuities

The sharp interruption in a uniform transmission line will lead to impedance mismatch and strongly disturb the transmission rate. Here, we apply the proposed concept to overcome the mismatch caused by the discontinuities of waveguide transmission lines. In Fig. 4(a), a rectangular waveguide with classical E-plane discontinuity (i.e., change in the height of the waveguide) is schematically presented. The operating frequency is $f_p = 200$ GHz. The background dielectric filling the waveguide has a relative permittivity of $\varepsilon_{\mathrm{WG}}^{\mathrm{act}} = 20$. The waveguide effective permittivity of the background dielectric is $\varepsilon_{\mathrm{WG}}^{\mathrm{eff}} = 1$ and the guided wavelength is $\lambda_g = 1500$ μm. The discontinuity of a stepped waveguide can be regarded as the load with an impedance of $Z_L = (0.24 + j\,0.41)Z_{\mathrm{WG}}$, where $Z_{\mathrm{WG}} = 50\ \Omega$ is the characteristic impedance of the input waveguide [higher waveguide in Fig. 4(a)].

To realize a match between Z_L and Z_{WG}, a parallel capacitor is required, corresponding to a WG-MTM element with a positive waveguide effective permittivity, $\varepsilon_E^{\mathrm{eff}}$. Through Eq. (2), we can calculate that the required element has an actual relative permittivity of $\varepsilon_E^{\mathrm{act}} = 62.4$ (i.e., $\varepsilon_E^{\mathrm{eff}} = 43.4$) and the thickness along the propagation direction of $\lambda_g/150$. Numerical results of sectional electric-field-magnitude distributions at f_p without and with the WG-MTM element are shown in Figs. 4(b) and 4(c), respectively. After adopting the matching network, the standing wave in Fig. 4(b) is completely removed and zero reflection is achieved, leading to uniform field distributions in the input and output waveguides. To demonstrate the matching performance of the network within a wide range of operating frequency, reflection coefficients are shown in Fig. 4(d). Numerical results indicate that the WG-MTM matching network significantly reduces the reflection at f_p from -3.6 to -47.3 dB and increases the -10-dB impedance bandwidth from 0% to 4.8% (i.e., from $0.985f_p$ to $1.034f_p$). Another classical waveguide discontinuity caused by the H-plane stepped-waveguide structure (i.e., change in the width of the waveguide) is also investigated, and a conceptual sketch is given in Fig. 4(e). The mismatch appears at the connection of the input waveguide and output waveguide and brings a load impedance of $Z_L = (0.32 + j\,0.45)Z_{\mathrm{WG}}$. Based on the proposed concept, we can utilize a single WG-MTM element

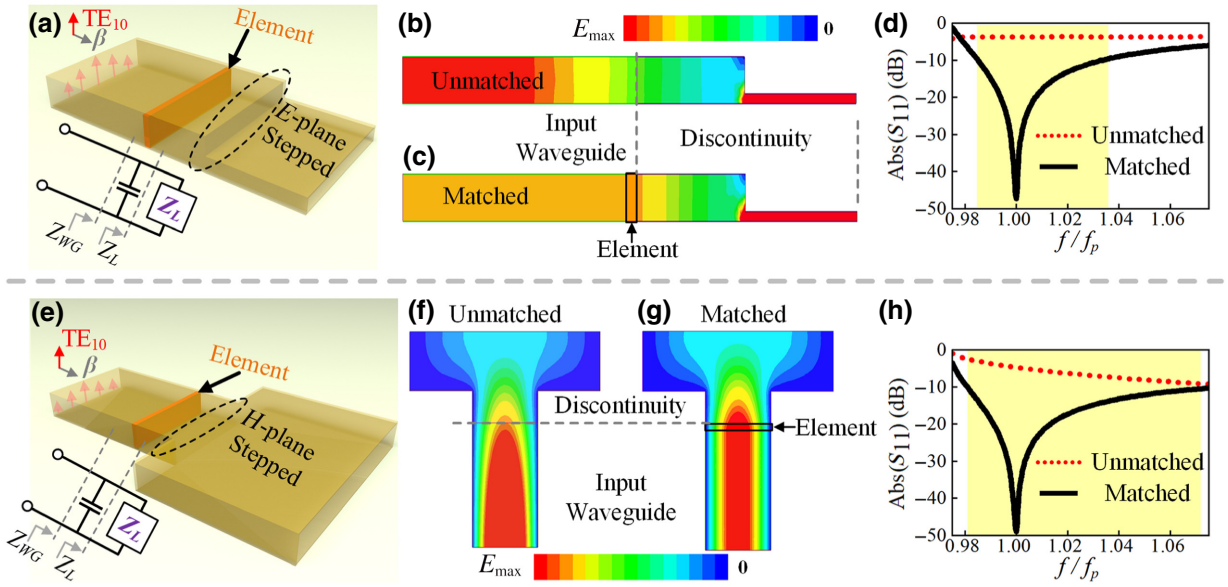

FIG. 4. Waveguide-metamaterial matching networks for transmission discontinuities. (a) Conceptual sketch of the network to match a waveguide with E-plane step (change in height). Distributions of electric field magnitude at f_p when the waveguide (b) contains or (c) does not contain the WG-MTM elements. (d) Simulated reflection coefficients when it is unmatched and matched. (e) Conceptual sketch of the network to match a waveguide with H-plane step (change in width). Distributions of electric field magnitude at f_p when the waveguide (f) contains or (g) does not contain the WG-MTM elements. (h) Simulated reflection coefficients when it is unmatched and matched.

that has a relative permittivity of $\varepsilon_E^{\text{act}} = 54.7$ (i.e., $\varepsilon_E^{\text{eff}} = 35.7$) and a thickness of $a = \lambda_g/150$ to cancel out the mismatch. As shown in Figs. 4(f) and 4(g), the electromagnetic wave can totally transmit from the input waveguide to the output waveguide with no reflection. Reflection coefficients in Fig. 4(h) reveal that the proposed network improves the reflection at f_p from -4.7 to -49.0 dB and increases the -10-dB impedance bandwidth from 0% to 9.8% (i.e., from $0.981f_p$ to $1.082f_p$). These two examples demonstrate that the proposed WG-MTM matching network has the potential for a transmission line with flexible structures. Detailed structures and dimensions of Figs. 4(a) and 4(e) are shown in Figs. S5 and S6 within the Supplemental Material [36].

B. Matching for active power amplifiers

Next, we turn our attention from passive transmission structures to active transmission structures. We take the power amplifier, which is a classical active device to convert a low-power signal into a high-power signal [37], as the second representative application of the proposed WG-MTM matching networks. Traditional power amplifiers are usually designed based on microstrip-type circuits and may suffer from higher radiation loss in millimeter-wave and terahertz domains due to their semiopen structures. However, the proposed WG-MTM networks with enclosed structures might reduce the effect of radiation loss and improve the performance.

In Figs. 5(a)–5(d), we present a conceptual sketch for the waveguide-integrated power amplifier. The gain of the signal is provided by the transistor. The input port and output ports of the transistor are connected with the top metallic surfaces of the input and output waveguide, respectively. The source impedance Z_{AP}^S and load impedance Z_{AP}^L of the amplifier must simultaneously satisfy a conjugate match, which means we must realize the match between $Z_{\text{AP}}^{S\,*}$ (conjugate impedance of Z_{AP}^S) and characteristic impedance of input waveguide, and the match between $Z_{\text{AP}}^{L\,*}$ (conjugate impedance of Z_{AP}^L) and characteristic impedance of output waveguide. In this example, the predesigned operating frequency is $f_p = 200$ GHz. We utilize a heterojunction bipolar transistor and two waveguides with a characteristic impedance of $Z_{\text{WG}} = 50\ \Omega$. The operating properties of the transistor are numerically studied using the commercial software Advanced Design System (ADS), and the power-supply voltage, V_{CC}, and bias current, I_{BB}, are set as 1.4 V and 60 μA, respectively. According to the load-pull and source-pull, the source and load impedances of the transistor for maximum power transfer are determined to be $Z_{\text{AP}}^{S\,*} = (9.8 - j\,6.2)\ \Omega$ and $Z_{\text{AP}}^{L\,*} = (33.2 - j\,15.6)\Omega$. Then, the input- and output-matching networks based on the concept of a waveguide metamaterial are developed to obtain the conjugate match. Sketches of the matching networks are presented in Figs. 5(b) and 5(d), and they both contain a single WG-MTM element, which is placed within the waveguide transmission line. For the input-matching network, the WG-MTM element

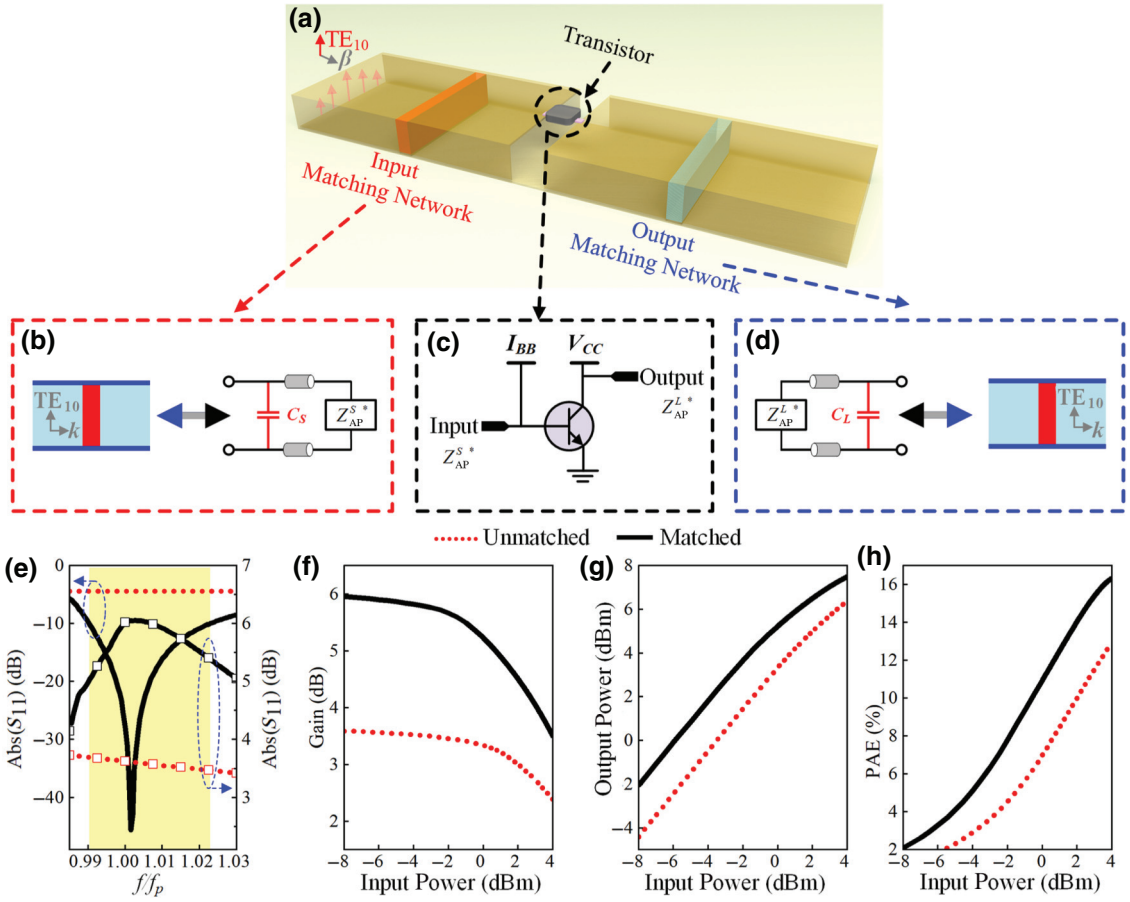

FIG. 5. Waveguide-metamaterial matching networks for the active power amplifier. (a) Sketch of the waveguide-integrated power amplifier, containing (b) input-matching network, (c) transistor with bias circuits, and (d) output-matching network. Matching network is composed of a single WG-MTM element integrated with the waveguide transmission line. (e)–(h) Performance comparisons before and after the proposed matching networks are inserted. (e) Reflection coefficient, (f) gain, (g) output power, and (h) PAE.

has a waveguide effective permittivity of $\varepsilon_E^{\text{eff}} = 16$ and a thickness of $a = 0.02\lambda_g$, and the length from Z_{AP}^{S} to the element is $0.077\lambda_g$. For the output-matching network, the WG-MTM element has a waveguide effective permittivity of $\varepsilon_E^{\text{eff}} = 5.5$ and a thickness of $a = 0.02\lambda_g$, and the length from Z_{AP}^{L} to the element is $0.17\lambda_g$. Through the cosimulation of ADS and the Ansoft high-frequency structure simulator (HFSS), the performances of the proposed waveguide-integrated power amplifier without or with the matching networks are studied. After adding the WG-MTM matching networks, the small-signal results in Fig. 5(e) illustrate that the reflection at f_p is significantly reduced from -4.4 to -49.5 dB, and the transmission achieves an increment of 2.4 dB (from 3.6 to 6.0 dB). The impedance of this structure is well matched from $0.99f_p$ to $1.022f_p$. Figures 5(f)–5(h) present the gain, output power, and power-added efficiency (PAE) versus the large-signal numerical analysis at f_p. The active performances of the proposed amplifier are also greatly improved with the aid of a waveguide metamaterial. For example, when the input power is -1 dBm, the gain, output power, and PAE have increments of 2.1 dB, 2.1 dB, and 3.8%, respectively. A detailed structure and dimensions of the proposed amplifier are shown in Fig. S7 within the Supplemental Material [36]. In Figs. 2–5, WG-MTM elements with high relative permittivities [e.g., 62.4 in Fig. 3(a) and 54.7 in Fig. 3(e)] can be realized by ceramic powders, which can provide dielectric constants ranging from 4.9 to 160 [38,39].

C. Matching for antennas

In the aforementioned applications, we mainly utilize the proposed WG-MTM matching networks to maximize the transmission property of an electromagnetic wave. It can also be exploited to enhance the radiation performance of an electromagnetic wave. Here, we adopt the proposed concept to address the mismatch issue of the antenna and improve its radiation property. The overall structure is schematically presented in Fig. 6(a). The example structure is composed of three parts: a waveguide-integrated cavity-slot antenna to radiate the electromagnetic wave, a microstrip line to excite the antenna, and a WG-MTM

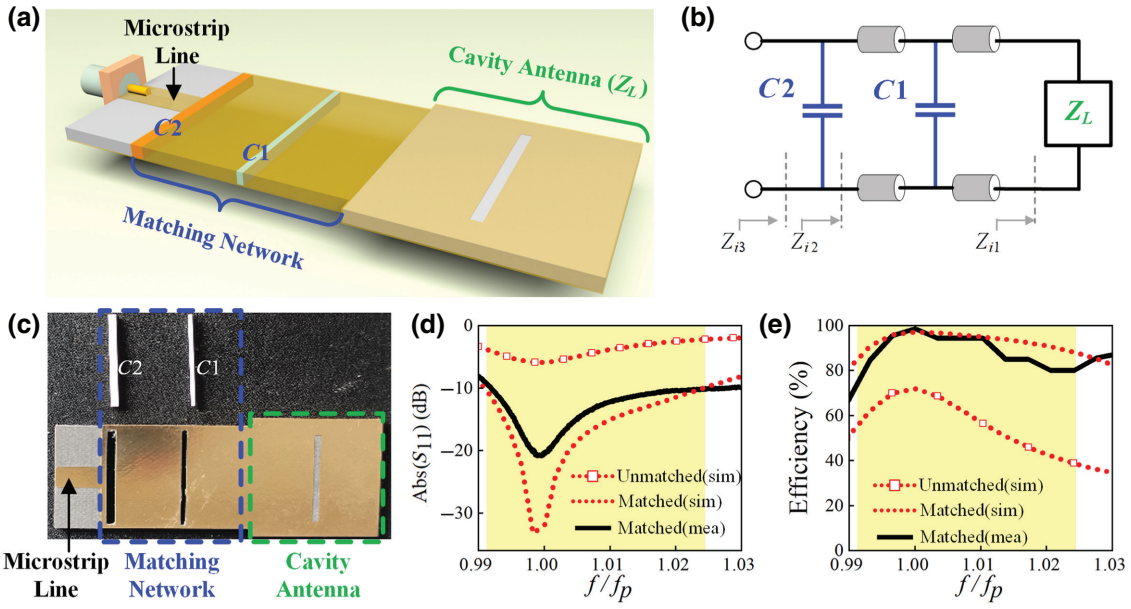

FIG. 6. Waveguide-metamaterial matching network for antenna. (a) Overall view of the structure to realize impedance matching for a cavity antenna by using a network with two WG-MTM elements. (b) Equivalent-circuit model of the proposed structure. (c) Photograph of the fabricated prototype of the cavity antenna with the proposed matching structure. Simulated and measured (d) reflection and (e) efficiency, when the cavity antenna is unmatched and matched.

matching network integrated with the waveguide. The predesigned frequency of the antenna is $f_p = 5.8$ GHz. The equivalent-circuit model of the structure is shown in Fig. 6(b). The antenna can be equivalent to a load with an impedance of $Z_L = (10.46 + j\,4.89)\ \Omega$ at f_p. The microstrip line can be equivalent to a source with an impedance of $Z_S = 50\ \Omega$. If the antenna is directly connected with the microstrip line, the mismatch between Z_L and Z_S would result in an obvious reflection and significant efficiency deterioration.

As shown in Figs. 6(a) and 6(b), we consider a matching network containing two WG-MTM elements equivalent to parallel capacitors ($C1$ and $C2$). According to the circuit theory, we derive that the network comprising a series reactance, $Z_{\text{series}} = (15.44j)\ \Omega$, and a parallel reactance, $Z_{\text{parallel}} = (-25.3j)\ \Omega$, can obtain a match between Z_L and Z_S. Subsequently, based on the concept of the waveguide metamaterial, the series reactance, Z_{series}, is realized by $C1$ and $\lambda_g/4$ waveguide transmission lines. $C1$ has a relative permittivity of $\varepsilon_E^{\text{act}} = 6.5$ and a thickness of $a = 0.0183\lambda_g$. The parallel reactance, Z_{parallel}, is realized by $C2$, which has a relative permittivity of $\varepsilon_E^{\text{act}} = 9.9$ and a thickness of $a = 0.0251\lambda_g$. To verify the performance of the designed matching network, a prototype of the whole structure is fabricated, as shown in Fig. 6(c). Two air cavities are etched on the waveguide dielectric board within which inserted WG-MTM elements are placed. $C1$ is fabricated using machinable glass ceramic and $C2$ is fabricated using 99.8% alumina. After filling the two air cavities with $C1$ and $C2$, we solder copper tapes on the top and bottom metal layers of the inserted regions to complete the metallic boundary of the waveguide. Numerical and experimental reflections and radiating efficiencies without and with the proposed network are depicted in Figs. 6(d) and 6(e). After adding the network, the experimental reflection at f_p is improved from -5.3 to -21 dB, and the -10-dB bandwidth is from $0.991f_p$ to $1.026f_p$. The radiation efficiency at f_p is significantly improved from 71.9% to 98.6%, with an increment of 26.7%, which implies that the proposed WG-MTM matching network enables the antenna to radiate almost all incident energy. Detailed dimensions of the structure, detailed values of gain, and radiation patterns are provided in Fig. S8 within the Supplemental Material [36]. Without loss of generality, examples in Figs. 4–6 utilize waveguides with background dielectrics that are not air. Moreover, it is also feasible to apply the theory of the WG-MTM to hollow rectangular waveguides with background dielectrics that are air (with an actual relative permittivity of 1). To verify this point, in Figs. S9 and S10 within the Supplemental Material [36], we present two examples that utilize the WG-MTM elements to match the transmission discontinuities of hollow rectangular waveguides.

IV. CONCLUSION

We demonstrate a general impedance-matching network based on waveguide metamaterial. The waveguide metamaterial can be systematically investigated to address problems regarding guide-wave impedance matching. The impedance properties of a waveguide metamaterial are

theoretically and numerically studied and verified, paving the way for the design of WG-MTM matching networks. Based on this concept, the network can be built by assembling WG-MTM elements under the guidance of an equivalent-circuit model. The feasibility of this concept is investigated through three representative implementations. Matching networks for waveguide transmission structures and an active power amplifier are verified through numerical simulations. A matching network for the cavity antenna is validated through experimental measurements. The proposed networks significantly improve the performances of these devices and exhibit merits of low loss, low crosstalk, high integration, and wide-applicable-frequency domains, promising exciting potential in various research fields.

ACKNOWLEDGMENTS

This work is supported by the National Natural Science Foundation of China (NSFC) under Grant No. 62022045 and in part by the Beijing Nova Program of Science and Technology under Grant No. Z191100001119082.

[1] H.-H. Hsiao, C. H. Chu, and D. P. Tsai, Fundamentals and applications of metasurfaces, Small Methods **1**, 1600064 (2017).
[2] M. Silveirinha and N. Engheta, Tunneling of Electromagnetic Energy through Subwavelength Channels and Bends Using ε-Near-Zero Materials, Phys. Rev. Lett. **97**, 157403 (2006).
[3] A. Haldar and A. O. Adeyeye, Artificial metamaterials for reprogrammable magnetic and microwave properties, Appl. Phys. Lett. **108**, 022405 (2016).
[4] G. Finocchio, O. Casablanca, G. Ricciardi, U. Alibrandi, F. Garescì, M. Chiappini, and B. Azzerboni, Seismic metamaterials based on isochronous mechanical oscillators, Appl. Phys. Lett. **104**, 191903 (2014).
[5] B. Assouar, B. Liang, Y. Wu, Y. Li, J.-C. Cheng, and Y. Jing, Acoustic metasurfaces, Nat. Rev. Mater. **3**, 460 (2018).
[6] N. Engheta, A. Salandrino, and A. Alu, Circuit Elements at Optical Frequencies: Nanoinductors, Nanocapacitors, and Nanoresistors, Phys. Rev. Lett. **95**, 095504 (2005).
[7] N. Engheta, Circuits with light at nanoscales: Optical nanocircuits inspired by metamaterials, Science **317**, 1698 (2007).
[8] Y. Sun, B. Edwards, A. Alu, and N. Engheta, Experimental realization of optical lumped nanocircuits at infrared wavelengths, Nat. Mater. **11**, 208 (2012).
[9] Y. Li, I. Liberal, and N. Engheta, Dispersion synthesis with multi-ordered metatronic filters, Opt. Express **25**, 1937 (2017).
[10] J.-S. Huang, T. Feichtner, P. Biagioni, and B. Hecht, Impedance matching and emission properties of nanoantennas in an optical nanocircuit, Nano Lett. **9**, 1897 (2009).
[11] U. K. Chettiar and N. Engheta, Metatronic transistor amplifier, Phys. Rev. B **92**, 165413 (2015).
[12] C. Walther, G. Scalari, M. I. Amanti, M. Beck, and J. Faist, Microcavity laser oscillating in a circuit-based resonator, Science **327**, 1495 (2010).
[13] Y. Li, I. Liberal, C. Della Giovampaola, and N. Engheta, Waveguide metatronics: Lumped circuitry based on structural dispersion, Sci. Adv. **2**, e1501790 (2016).
[14] W. Rotman, Plasma simulation by artificial dielectrics and parallel-plate media, IRE Trans. Antennas Propag. **10**, 82 (1962).
[15] C. Della Giovampaola and N. Engheta, Plasmonics without negative dielectrics, Phys. Rev. B **93**, 195152 (2016).
[16] Y. Li and Z. Zhang, Experimental Verification of Guided-Wave Lumped Circuits Using Waveguide Metamaterials, Phys. Rev. Appl. **9**, 044024 (2018).
[17] F. R. Prudencio, J. R. Costa, C. A. Fernandes, N. Engheta, and M. G. Silveirinha, Experimental verification of 'waveguide' plasmonics, New J. Phys. **19**, 123017 (2017).
[18] Y. Li, I. Liberal, and N. Engheta, Structural dispersion-based reduction of loss in epsilon-near-zero and surface plasmon polariton waves, Sci. Adv. **5**, eaav3764 (2019).
[19] X. Qin, W. Sun, Z. Zhou, P. Fu, H. Li, and Y. Li, Waveguide effective plasmonics with structure dispersion, Nanophotonics **11**, 1659 (2022).
[20] D. M. Pozar, in *Microwave Engineering* (John Wiley & Sons, New York, 1998), 2nd ed..
[21] Z. Zhou, Y. Li, E. Nahvi, H. Li, Y. He, I. Liberal, and N. Engheta, General Impedance Matching via Doped Epsilon-Near-Zero Media, Phys. Rev. Appl. **13**, 034005 (2020).
[22] Y. Li, Z. Zhang, W. Chen, Z. Feng, and M. F. Iskander, A switchable matching circuit for compact wideband antenna designs, IEEE Trans. Antennas Propag. **58**, 3450 (2010).
[23] H. F. Pues and A. R. Vandecapelle, An impedance-matching technique for increasing the bandwidth of microstrip antennas, IEEE Trans. Antennas Propag. **37**, 1345 (1989).
[24] A. Chen and F. Monticone, Active scattering-cancellation cloaking: Broadband invisibility and stability constraints, IEEE Trans. Antennas Propag. **68**, 1655 (2020).
[25] A. Tittl, M. G. Harats, R. Walter, X. Yin, M. Schaeferling, N. Liu, R. Rapaport, and H. Giessen, Quantitative angle-resolved small-spot reflectance measurements on plasmonic perfect absorbers: Impedance matching and disorder effects, ACS Nano **8**, 10885 (2014).
[26] P. Spinelli, M. Hebbink, R. de Waele, L. Black, F. Lenzmann, and A. Polman, Optical impedance matching using coupled plasmonic nanoparticle arrays, Nano Lett. **11**, 1760 (2011).
[27] X. Li, W. Chen, P. Zhou, Y. Wang, F. Huang, S. Li, J. Chen, and Z. Feng, A 250–310 GHz power amplifier with 15-dB peak gain in 130-nm SiGe BiCMOS process for terahertz wireless system, IEEE Trans. Terahertz Sci. Technol. **12**, 1 (2022).
[28] C. Shi, X. Zang, Y. Wang, L. Chen, B. Cai, and Y. Zhu, A polarization-independent broadband terahertz absorber, Appl. Phys. Lett. **105**, 031104 (2014).
[29] Y. Cui, K. H. Fung, J. Xu, H. Ma, Y. Jin, S. He, and N. X. Fang, Ultrabroadband light absorption by a sawtooth anisotropic metamaterial slab, Nano Lett. **12**, 1443 (2012).
[30] D. Ye, Z. Wang, K. Xu, H. Li, J. Huangfu, Z. Wang, and L. Ran, Ultrawideband Dispersion Control of a

Metamaterial Surface for Perfectly-Matched-Layer-Like Absorption, Phys. Rev. Lett. **111**, 187402 (2013).

[31] A. H. Dorrah, M. Chen, and G. V. Eleftheriades, Bianisotropic Huygens' metasurface for wideband impedance matching between two dielectric media, IEEE Trans. Antennas Propag. **66**, 4729 (2018).

[32] K. Im, J.-H. Kang, and Q. H. Park, Universal impedance matching and the perfect transmission of white light, Nat. Photonics **12**, 143 (2018).

[33] R. E. Collin, in *Field Theory of Guided Waves* (John Wiley & Sons, New York, 1990), 2nd ed.

[34] S. A. Schelkunoff, Impedance concept in wave guides, Q. Appl. Math. **2**, 1 (1944).

[35] L.-S. Wu, B. Xia, J. Mao, and W.-Y. Yin, A half-mode substrate integrated waveguide ring for two-way power division of balanced circuit, IEEE Microw. Wireless Compon. Lett. **22**, 333 (2012).

[36] See the Supplemental Material at http://link.aps.org/supplemental/10.1103/PhysRevApplied.18.034070 for numerical calculations and experimental setup, detailed geometries of simulated and fabricated structures, and additional discussions about the proposed approach.

[37] X. Li, W. Chen, Y. Wang, and Z. Feng, 180 GHz high-gain cascode power amplifier in a 130 nm SiGe process, Electron. Lett. **56**, 498 (2020).

[38] Z. Zhou, Y. Li, H. Li, W. Sun, I. Liberal, and N. Engheta, Substrate-integrated photonic doping for near-zero-index devices, Nat. Commun. **10**, 4132 (2019).

[39] Z. Zhou and Y. Li, A photonic-doping-inspired SIW antenna with length-invariant operating frequency, IEEE Trans. Antennas Propag. **68**, 5151 (2020).